A Magnetically Actuated Variable Stiffness Manipulator Based on Deployable Shape Memory Polymer Springs

*Theodosia Lourdes Thomas, Jonathan Bos, Juan J. Huaroto, Venkatasubramanian Kalpathy Venkiteswaran, and Sarthak Misra**

Continuum manipulators have found several applications in surgical interventions like endoscopy, laparoscopy, and as end-effectors for surgical robots. Continuum manipulators coupled with magnetic actuation can be precisely maneuvered inside the human body. Recently, variable stiffness manipulators (VSMs) have been introduced for enhanced dexterity and safe navigation. This study presents a new design of a magnetically actuated VSM based on shape memory polymer (SMP) springs. The VSM has a silicone backbone enclosed within a spring made of SMP that can change in length with stiffness change that is triggered by Joule heating. The stiffness and thermal characteristics of the VSM are studied using analytical models and experiments. Subsequently, a one-segment VSM and a two-segment VSM having outer diameters of 9 and 10 mm and lengths of 15 and 25 mm, respectively, capable of extending to four times their length are designed. The VSM can be deployed in a compact form and extended to achieve variable bending curvatures in soft and rigid states, which can facilitate instrument insertion and reduce operation invasiveness. Potential clinical applications are demonstrated by incorporating miniature camera, biopsy tool, and laser optical fiber in the working channel of the VSM and coupled with robotic magnetic actuation.

1. Introduction

The last few years have seen a rapid growth in the application of continuum manipulators in diverse fields ranging from space and deep-sea explorations to minimally invasive surgical interventions.[1] The design of continuum manipulators inspired from nature emulates the flexibility of the body of a snake, the tentacles of an octopus, among others. Such manipulators composed of elastic components with infinite degrees of freedom can adapt their shape and operate in confined spaces.[2] A great deal of previous research in continuum manipulators has focused on tendon-driven manipulators, concentric tube manipulators, and multibackbone manipulators.[3] Although such manipulators with extrinsic actuation embody high flexibility, they are affected by friction and backlash caused by cables, torsion, and snapping behavior of concentric tube designs.[4,5] Continuum manipulators based on compliant mechanisms have several advantages as they are monolithic in nature which lead to easy fabrication, and with the elimination of friction, backlash, and noise, there is no need for lubrication.[6] However, these mechanisms are affected by fatigue and the input–output relationship is perturbed by energy storage.[7]

Minimally invasive surgery (MIS) is an increasingly important application of interest within the field of continuum manipulators.[4] MIS requires only small incisions to perform the surgery on the patient, reduces the operating time, and leads to fast recovery. Continuum manipulators can improve MIS by reaching difficult-to-access surgical sites with high dexterity and accuracy. With the rapid advances in the field of robot-assisted surgery, continuum manipulators are increasingly being used as end-effectors for dexterous manipulation of the surgical tools inside the human body, and complement the capabilities of the surgeon. There is a growing trend toward the design of soft continuum manipulators, which can adapt and be gently maneuvered in a constrained environment in the vicinity of various objects.[8] For example, Kim et al. demonstrated a ferromagnetic soft continuum robot that can be steered through complex phantom vasculature, while growing hydrogel skin on its surface that significantly reduces friction.[9] Magnetically actuated soft manipulators have great potential in creating miniaturized designs made by embedding ferromagnetic particles in soft polymer composites or incorporating small permanent magnets, which can then be controlled remotely with the application of external magnetic fields.[10,11] While soft manipulators have proven good

T. L. Thomas, J. Bos, J. J. Huaroto, V. Kalpathy Venkiteswaran, S. Misra
Surgical Robotics Laboratory
Department of Biomechanical Engineering
University of Twente
7500 AE Enschede, The Netherlands
E-mail: s.misra@utwente.nl

S. Misra
Surgical Robotics Laboratory
Department of Biomedical Engineering
University of Groningen and University Medical Centre Groningen
9713 GZ Groningen, The Netherlands

The ORCID identification number(s) for the author(s) of this article can be found under https://doi.org/10.1002/aisy.202200465.

**ADVANCED
SCIENCE NEWS**

www.advancedsciencenews.com

**ADVANCED
INTELLIGENT
SYSTEMS**
Open Access

www.advintellsyst.com

maneuverability, rigidity is essential for higher motion accuracy and to exert forces.[12] Both rigidity and softness are desirable attributes for surgical functions which is useful, for instance, during deployment of laparoscopy tools, and performing biopsy.

Variable stiffness in surgical manipulators has been gaining significant attention in recent years. Several studies have investigated different mechanisms to achieve variable stiffness such as granular/particle jamming, antagonistic arrangement of actuators, and stimuli-responsive stiffness-tunable materials.[13] A variable stiffness mechanism based on fiber jamming transition was introduced in the STIFF-FLOP soft manipulator to provide stability to its distal module by making it rigid, however miniaturization of this technology proved to be challenging.[14] A lightweight reconfigurable stiffness-changing skin based on layer jamming was created and adopted as on-demand joints for a continuum manipulator enabling dynamic adjustment of the operating workspace.[15] Cable-driven actuators[16] and fluidic actuators[17] are commonly used in antagonistic methods, but are limited by low range of stiffness variation and controllability when it comes to MIS.[18]

Stiffness-tunable materials such as low melting point alloys (LMPAs), shape memory alloys (SMAs), and shape memory polymers (SMPs) can attain significant stiffness change.[19–23] Despite the toxic nature of LMPA, owing to its transition speed, it has been used in the multisegment designs of a cable-driven continuum manipulator for MIS application,[20] and magnetic variable stiffness catheters for applications in cardiac ablation and robotic ophthalmic surgery.[21,24] SMAs have high power-to-weight ratio, are biocompatible, easy to miniaturize, and can be activated using Joule heating.[25] Therefore, SMA wires in the form of springs, strips, and wavy patterns have been used in the design of continuum manipulators for actuation and variable stiffness.[22,26,27] However, SMAs exhibit relatively lower range of stiffness change than SMPs, a limitation that could be solved by combining with a thermoplastic.[28] SMPs are versatile due to their compatibility with 3D printing and multimaterial fabrication. Material synthesis enables developing multi-SMP, that is, SMP with two or more transition temperatures, manifesting improved mechanical properties and recoverability.[29,30] Recently, SMP was used in the design of magnetic variable stiffness catheters in which graphite, neodymium, and carbon black particles were incorporated in the SMP composite to improve the electrical and thermal conductive properties.[23,31]

This work presents a new design of a magnetically actuated variable stiffness manipulator (VSM) based on SMPs. The VSM is composed of a silicone lumen enveloped by a helix-shaped spring made of SMP and a permanent magnet attached to its tip. The SMP spring with an embedded resistive wire is fabricated by following a novel process of retraining the SMP to alter its primary shape. The working principle of the VSM relies on phase change property of SMP for shape fixity in conjunction with magnetic fields for actuation. The VSM demonstrates shape fixity or shape locking capability, that is, the shape of the VSM can be fixed during magnetic actuation to resist external forces. Moreover, the VSM made of an extensible SMP spring can attain a compact form in its compressed form and operate in various configurations of extendable lengths. The modularity of the VSM as a two-segment VSM (with a central working channel to accommodate laparoscopic tools) is also

demonstrated to achieve different bending curvatures with selective shape locking capability. The major contributions of this work are as follows: 1) design and fabrication of a deployable and modular VSM that is magnetically actuated and exhibits variable stiffness with variable working length; 2) shape locking capability of VSM that has potential to facilitate insertion and act as a stabilizer while deploying laparoscopic tools; 3) stiffness and thermal characterization of VSM using analytical models and experiments; and 4) clinical feasibility demonstration for applications in endoscopy, biopsy, and laser surgery using robot-assisted magnetic actuation.

2. Results and Discussion

2.1. Design

The VSM has a backbone made of a silicone tube enclosed within a spring made of SMP and a permanent ring magnet attached to its tip. The SMP spring is embedded with a resistive wire to heat the SMP by passing current. The SMP spring in rigid phase is initially in a compressed state resulting in a minimum length of the VSM, and it can be moved to a target location in its compact form. When the SMP is activated by heating, it transitions to the soft phase and by pushing the silicone tube, the VSM is extended in length. The orientation of the VSM tip with magnet is controlled with the application of a bending moment resulting from external magnetic fields. The VSM can be deflected to extend or bend while the SMP is in soft phase, and its shape can be fixed when the SMP transitions to rigid phase. A two-segment design of the VSM can be formed using two SMP springs in series enclosing a two segment concentric tube backbone of silicone (**Figure 1**a). Various bending configurations can be achieved with selective activation, bending, and extension of the VSM segments (Figure 1b). The stiffness change of the SMP when transitioning between the soft and rigid phases enables fixing the shape of the VSM (Figure 1c), which is controlled under magnetic actuation.

2.2. Stiffness Characterization

The shape fixity of the VSM, that is, the ability of the VSM to retain the temporary shape upon removal of mechanical deformation, is crucial for the design. This is achieved by designing the VSM to have high stiffness in the glass phase of SMP when it becomes rigid and low stiffness in the rubber phase of SMP when it becomes soft. As inferred from Figure 1c, the elastic modulus of the SMP in glass phase ($E_g = 1000 \, \text{MPa}$) drops by three orders of magnitude when transitioning to rubber phase ($E_r = 1 \, \text{MPa}$). Hence, maximizing the bending rigidity of the SMP spring in glass phase is prioritized. The SMP spring can be modeled as a cantilever beam with bending rigidity (β) given by[32]

$$\beta = \frac{Eld^4}{64nr(2+\nu)} \tag{1}$$

where E and ν are the elastic modulus and Poisson's ratio of SMP at a given phase, respectively; d, l, r, and n are the diameter of the spring wire, length, mean coil radius, and number of active coils
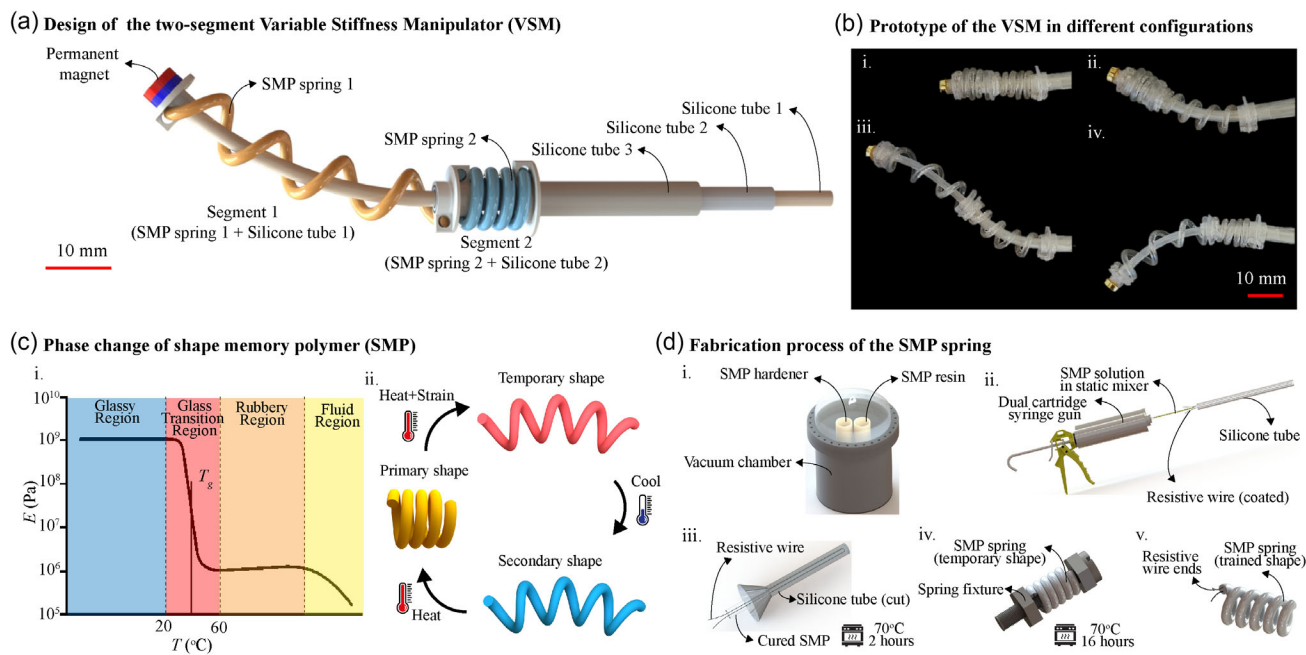
Figure 1. a) An illustration of the design of the two-segment VSM. b) Fabricated prototype of the VSM in different bending and extension configurations. c) Phase change of SMP: i) Plot of elastic modulus (E) versus temperature (T) of the SMP with glass transition temperature (T_g), adapted from.[47] ii) Shape memory effect illustrated for a SMP spring. d) Fabrication process of the SMP spring: i) Vacuum drying of the SMP resin and hardener for 2 h. ii) Injection of the mixed SMP solution into a silicone tube with a coated resistive wire. iii) Curing of the silicone mold in an oven at 70 °C for 2 h and demolding the cured SMP from the silicone mold. iv) Fixing the SMP wire into a temporary shape of the spring and training the SMP spring in the oven 2 cycles of 70 °C for 16 h. v) The trained SMP spring.

of the spring, respectively. The lateral deflection (θ) of the VSM caused by a pure bending moment (M) is given by

$$\theta = \frac{ML}{(\beta + E_s I_s)} \tag{2}$$

where E_s and I_s are the elastic modulus and area moment of inertia of the silicone tube, and L is the length of the VSM. The lateral deflection of the VSM as a function of mean coil radius and spring wire diameter is shown in **Figure 2**a. For high stiffness, that is, high bending rigidity given by Equation (1), 3 mm mean coil radius and 2 mm spring wire diameter are chosen considering the fabrication limitations. The number of active coils of the SMP spring and length of the VSM are determined by analyzing the resulting bending rigidity of the VSM composed of the SMP spring and silicone tube. To retain the shape fixity for a given length of VSM, the bending rigidity of the SMP spring (β) should be dominant over that of the silicone tube ($E_s I_s$). The suitable design region can be ascertained from Figure 2b, for lengths after the intersection of the plot lines of SMP spring and silicone tube.

Three VSMs with different combinations of length, number of active coils, size of silicone tubes, and magnets are designed. The lateral deflection of the VSMs in glass and rubber phases are analyzed with the application of a bending moment resulting from the magnetic fields (Figure 2d,e, Video S1, Supporting Information). Experiments are conducted in compressed and different extended lengths of the VSMs (Figure 2f). The theoretical model agrees better with the experimental results for small

deflections (<10°) in glass phase than for large deflections in rubber phase. This can be attributed to the ambiguity in the elastic modulus of the SMP as it transitions from the glass transition range to the fully rubber region and the geometric nonlinearities due to large deflection.

Based on the results, VSM-2 and VSM-3 having 4.5 and 5.5 active coils are chosen over VSM-1 having 3.5 active coils as the final designs as these demonstrate less deflection in glass phase (Figure 2c). VSM-2 and VSM-3 have compressed lengths of 13 and 15 mm, and an extended working lengths of 50 and 70 mm, respectively. For demonstration of VSM functions, a one-segment VSM is fabricated using VSM-3 design and a two-segment VSM is fabricated using a combination of two VSM-2 designs. Both the one-segment and the two-segment VSM designs in their respective fully extended lengths are capable of bending up to an angle of 180° in rubber phase while using a magnetic field of 70 mT. The different shapes of the two-segment VSM are captured by selectively heating each of the segments, extending to various lengths and deflecting to various bending curvatures with the application of magnetic fields of 40 mT (Figure 2g).

2.3. Thermal Actuation

The variable stiffness in the VSM is activated by means of Joule heating. The SMP used in the design has a glass transition temperature of 35 °C, below which it is in glass phase and at 60 °C it reaches the rubber phase. The SMP spring wire is embedded
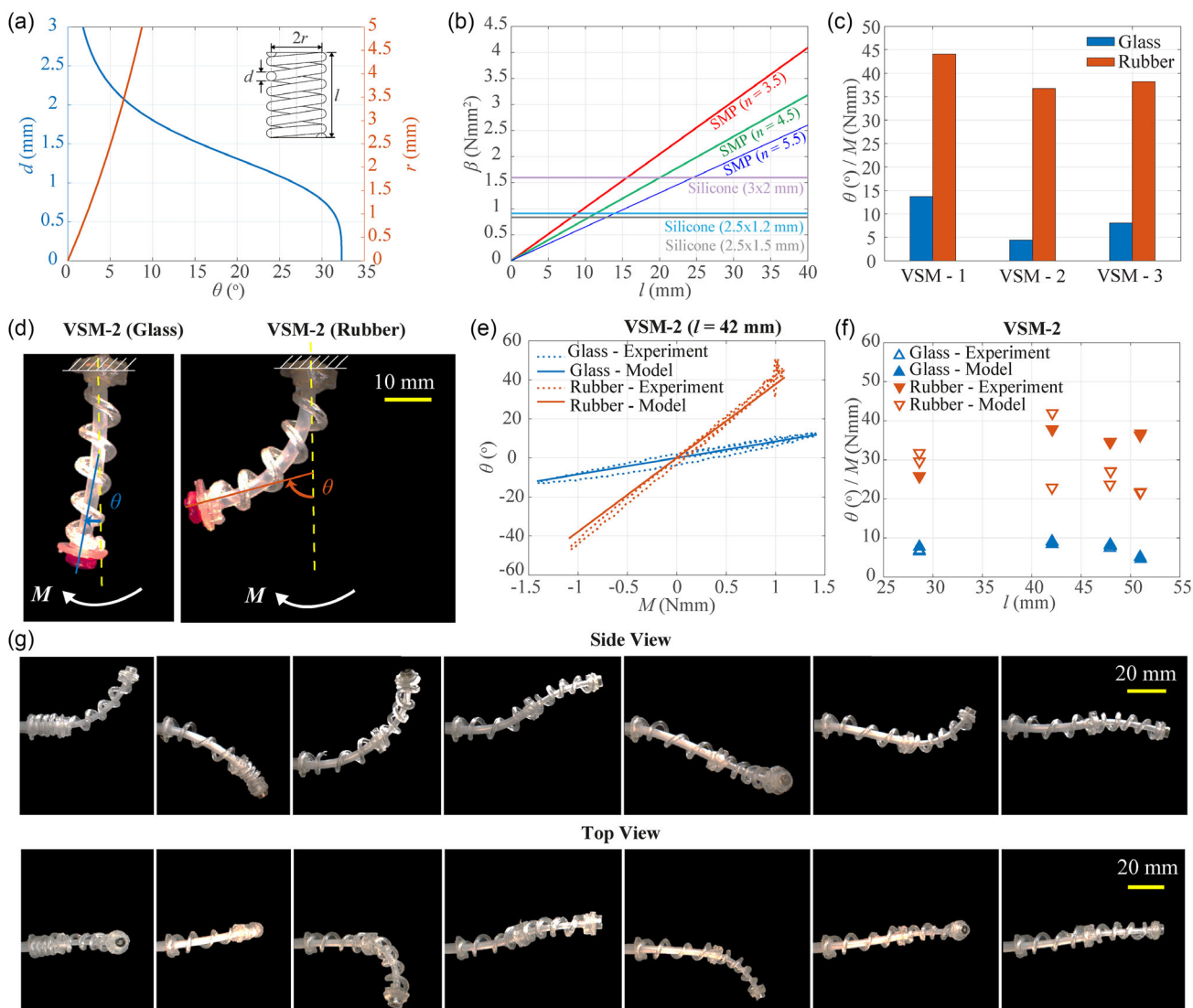
Figure 2. a) Effect of wire diameter (*d*) and mean coil radius (*r*) of the spring on its lateral deflection (*θ*). b) Bending rigidity (*β*) for different lengths of the SMP springs with *n* active coils and silicone ($D_o \times D_i$) tubes of outer diameter (D_o) and inner diameter (D_i). c) The degree of lateral deflection (*θ*) over the bending moment (*M*) in glass and rubber phases for three designs of VSM: VSM-1 ($n = 3.5$, $l = 35$ mm, $D_o = 2.5$ mm, $D_i = 1.2$ mm); VSM-2 ($n = 4.5$, $l = 51$ mm, $D_o = 3$ mm, $D_i = 2$ mm); VSM-3 ($n = 5.5$, $l = 45$ mm, $D_o = 2.5$ mm, $D_i = 1.5$ mm). d) *θ* of VSM-2 in glass and rubber phases for the same magnetic bending moment (*M*) generated by external magnetic fields. e) *θ* versus *M* relationship calculated by the cantilever beam model and measured by the experiments with VSM-2 of length ($l = 42$ mm). f) The degree of *θ* over *M* in glass and rubber phases for VSM-2 design with different working lengths (*l*). g) Different bending shapes of the two-segment VSM design at varying lengths with the application of magnetic fields captured as side and top views.

with a nichrome wire of diameter 0.12 mm running through the cross section of the SMP spring wire twice, with the two ends of the nichrome wire leaving the end of the SMP spring wire to connect to a power supply. The cross section of the SMP spring wire is composed of two circular sections of the nichrome wire (running in two directions) surrounded by the SMP layer. The overall design can be approximated by a cross section composed of single section of nichrome wire having an effective radius of two wires and surrounded by the SMP layer (**Figure 3**b). As current flows through the nichrome wire, the temperature of the surrounding SMP increases. Assuming a cylindrical coordinate

system with the center of the cross section as origin and temperature varies along the radial direction, the rise in temperature is modeled using the 1D transient heat transfer equation[33] given by

$$\frac{\partial T}{\partial t} = a_o \left(\frac{\partial T}{\partial r} \frac{1}{r} + \frac{\partial^2 T}{\partial r^2} \right) \tag{3}$$

with an initial condition

$$T(r, 0) = T_0, \quad (r_1 \leq r \leq r_2) \tag{4}$$

**ADVANCED
SCIENCE NEWS**

www.advancedsciencenews.com

**ADVANCED
INTELLIGENT
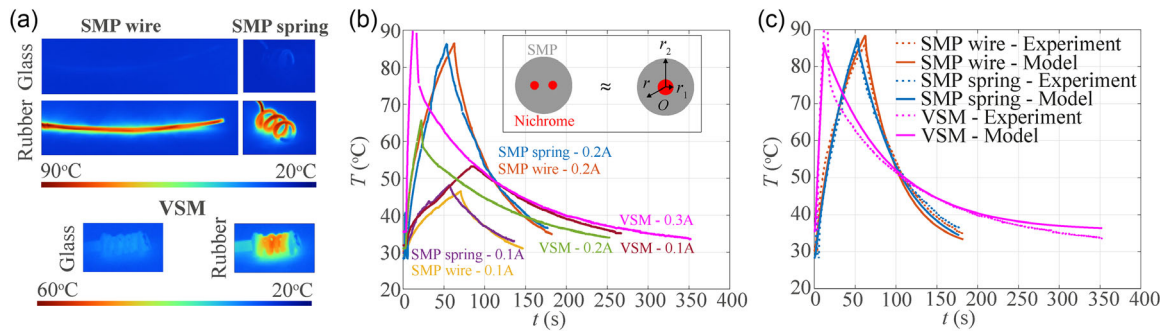SYSTEMS**

www.advintellsyst.com

Figure 3. a) Thermal camera images showing the glass and rubber phases of the SMP wire, SMP spring, and the VSM. b) The temperatures (T) measured by the thermal camera over time (t) at applied currents of 0.1, 0.2, and 0.3 A. The inset depicts the cross section of the samples composed of SMP (gray) and nichrome (red), and the approximation of the two nichrome wire parts as a single part for the heat transfer model. A cylindrical coordinate system is fixed with origin (O) at the center of the cross section, r_1 is the effective radius of nichrome and r_2 is the radius of SMP, and r is any point radius in the SMP layer. c) The temperatures estimated by the heat transfer model and measured by the thermal camera for the SMP wire at 0.2 A, SMP spring at 0.2 A, and the VSM at 0.3 A.

and the boundary conditions

$$I^2 R = 2\pi r \lambda_0 \frac{\partial T}{\partial r}, \quad (r = r_1) \tag{5}$$

$$\lambda_0 \frac{\partial T}{\partial r} = h(T - T_0), \quad (r = r_2) \tag{6}$$

Here, T and T_0 are the temperatures of the SMP layer and the ambient temperature, respectively; t is the time, r_1 is the effective radius of the two nichrome wires, r_2 is the radius of the SMP layer, and r is any point radius in the SMP layer. The thermal diffusivity of nichrome is given by $a_0 = \lambda_0/(\rho_0 c)$, where λ_0, ρ_0, and c are the thermal conductivity, density, and specific heat capacity of nichrome, respectively. i, R, h are the current, the resistance of the nichrome wire, and the surface heat transfer coefficient of the SMP with air, respectively.

The heating and cooling behavior of the VSM upon actuation are analyzed by measuring the temperature using an infrared camera. The straight SMP wire before training, the SMP spring, and the VSM are tested. Temperatures are measured between the transition from glass to rubber phase, and vice versa, with the application of currents in the range 0.1–0.3 A. The thermal camera images (Video S2, Supporting Information), temperatures of the samples measured by the infrared camera, and the temperatures calculated by the heat transfer model (Equation (3)) are shown in Figure 3. Results show a good agreement between the model estimated and experimentally measured temperatures. It takes 20 s to thermally actuate the VSM and reach rubber phase (60 °C) while using a current of 0.2 A, and 230 s to cool the VSM and reach glass phase (30 °C) at room temperature.

It is to be noted that this work is a proof-of-concept study using a polyurethane SMP with phase change that occurs between 35 and 60 °C. This temperature range can be challenging for clinical applications as the human body temperature is typically 36–37 °C, and prolonged exposure to higher temperatures can cause thermal damage to tissue.[34] In the experiments here, the cooling time is long owing to the natural convection cooling process of the VSM that takes place in air. It can be reduced if operating in fluid or with the inclusion of an active cooling

element.[21] Moreover, the development and usage of SMPs with phase transition taking place within a smaller range of temperatures while exhibiting a wider range of stiffness change can reduce cooling time, and in turn can improve the response time of the VSM.[35–37]

2.4. Applications

Potential clinical applications of the VSM as a steerable surgical manipulator are demonstrated with one-segment and two-segment designs. A permanent magnet attached to the end-effector of a robotic arm is programmed to generate the required magnetic field to control the VSM. The one-segment VSM is used to demonstrate endoscopy and biopsy procedure in a stomach phantom having polyps. Stomach polyps are abnormal tissue growth found in the inner lining of the stomach, which maybe causes no external symptoms and can sometimes be cancerous if left untreated.[38] The polyps are detected during an endoscopy procedure in which a long flexible tube equipped with a miniature camera at the end is inserted via the mouth, through the esophagus, and into the stomach for visual examination. A polyp can be removed for inspection by inserting a biopsy forceps or snare.

In the first experiment, a miniature camera (0.91 mm in diameter) is integrated in the working channel of the one-segment VSM and tested in a stomach phatom. The one-segment VSM is inserted through the esophagus in its compressed form while in glass phase phase, and upon entering the stomach the VSM is extended in length by activating the SMP to rubber phase. The VSM is deflected in rubber phase with the application of magnetic fields using the robot arm while manually controlling its length to scan the volume of the stomach and detect the three polyps. **Figure 4**a depicts the endoscopy procedure carried out by the one-segment VSM and the view through the miniature camera of the polyps inside the stomach (Video S3, Supporting Information). In the second experiment, a cold snare polypectomy tool is integrated in the working channel of the one-segment VSM. As shown in Figure 4b, the one-segment VSM is inserted to reach the polyp similar to the first experiment.
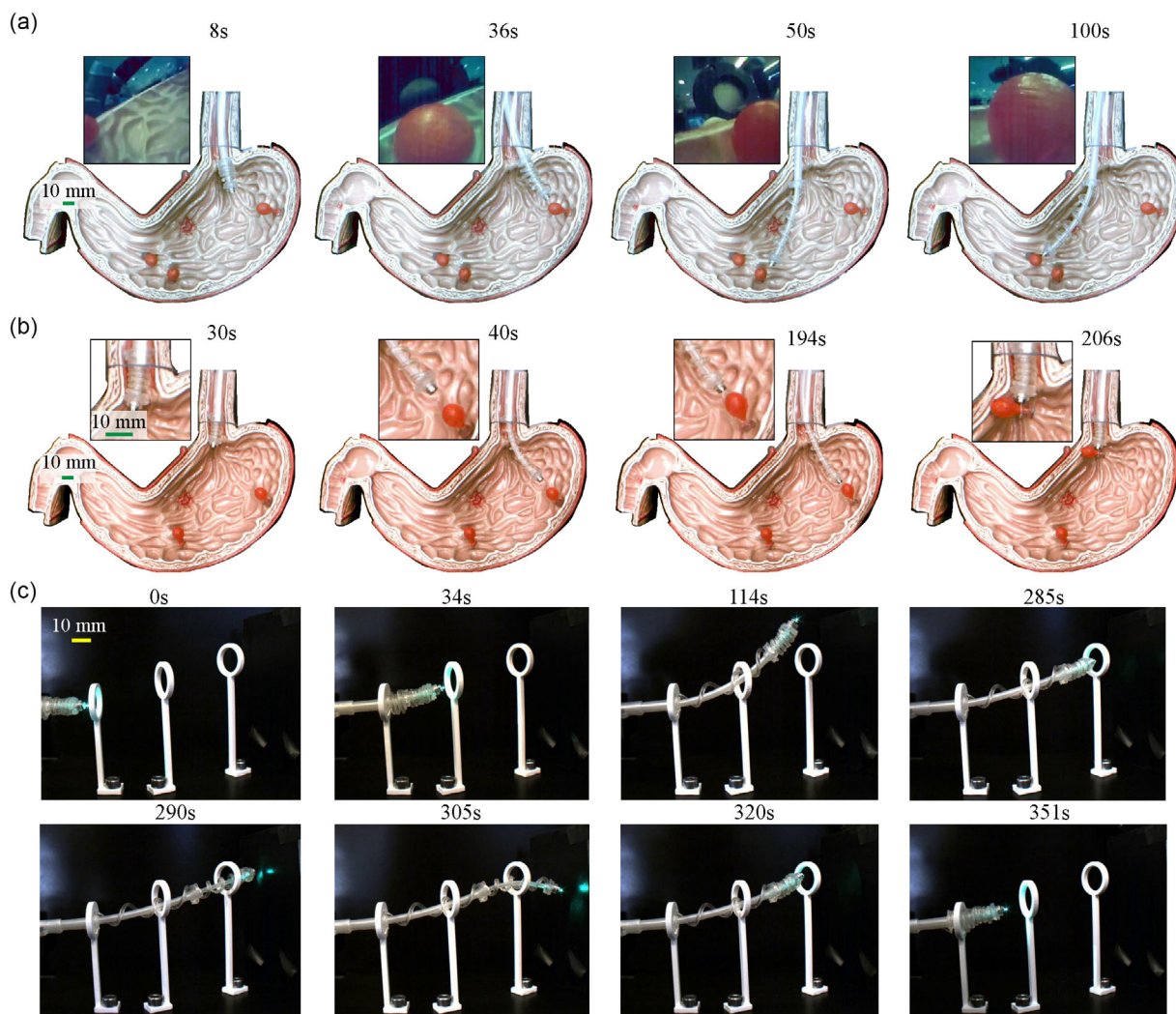
Figure 4. Demonstration of endoscopy, biopsy, and laser ablation applications of the VSM: a) one-segment VSM integrated with a miniature camera guided inside a stomach phantom using robotic magnetic actuation to detect the three polyps. The inset shows the miniature camera view. b) One-segment VSM integrated with a cold snare removes one of the polyps in the inner lining of the stomach. The inset shows a magnified view of the VSM. c) Two-segment VSM integrated with an optical fiber carrying laser light is steered to navigate through three rings oriented in 3D space.

Thereafter, the VSM is locked in position using the magnetic field while the SMP transitions to glass phase, and the snare is deployed to grasp the polyp. The polyp is resected by retracting the snare, and the SMP is activated to rubber phase. Thereafter, the VSM is retracted back to its compressed form for subsequent withdrawal through the esophagus (Video S4, Supporting Information).

The maneuverability and shape fixity of the two-segment VSM is demonstrated by navigating it through three rings distinctly oriented in 3D (Video S5, Supporting Information). An optical fiber is integrated in the working channel of the VSM to transmit laser light. As shown in Figure 4c, the VSM enters the first ring in its compact form, in which both the distal and proximal segments known as segments 1 and 2, respectively, as indicated in Figure 1a, are in fully compressed states while in glass phase. The SMP spring in segment 2 is activated by heating, as it transitions to rubber phase the VSM is deflected with the application

of magnetic field to align the tip with the second ring. Subsequently, segment 2 is extended in length by pushing silicone tube 2 to pass through the second ring, and the VSM is deflected again to align the tip to the third ring. Thereafter, segment 2 is cooled to transition the SMP to glass phase, consequently locking the shape of the VSM. Thereon, segment 1 is activated by heating, and with the transition to rubber phase it is extended in length by pushing silicone tube 1 to pass through the third ring. While in the current phase of glass segment 2 and rubber segment 1, the tip of the VSM is further deflected by bending segment 1 to point the laser beam on a black screen located in the vicinity. The VSM is retracted back through the three rings following the whole process in reverse order. This demonstration shows the uncoupled actuation, bending, and shape locking capability of the two-segment VSM while navigating a restricted environment and transporting laser beam as a potential application for laser surgery.

**ADVANCED
SCIENCE NEWS**

www.advancedsciencenews.com

**ADVANCED
INTELLIGENT
SYSTEMS**
Open Access

www.advintellsyst.com

The focus of this work is in maximizing the shape fixity of the VSM by designing SMP spring with optimal dimensions, which has proven to be effective in the above demonstrations. It is worth mentioning that a very small deflection or bounce back of the SMP segment might occur as it becomes rigid. The amount of bounce back depends on broadly three factors: shape fixity of SMP material, fabrication process, and overall design.[39,40] For the VSM design proposed here, the silicone tube and integrated laparoscopic tools will also contribute to this effect. Therefore, it is challenging to estimate the exact amount of bounce back of the VSM owing to the convoluted factors of SMP fixity and design dependency. However, it is safe to say that the bounce back is minimal and does not significantly affect manipulation, especially under controlled magnetic actuation as shown in the biopsy and the laser surgery demonstrations (Video S4 and S5, Supporting Information). For future clinical translation, commercially available systems such as Stereotaxis Niobe magnetic navigation system (Stereotaxis, USA) and Aeon Phocus (Aeon Scientific AG, Switzerland) can be used for the magnetic actuation of the VSM.[41,42] Furthermore, the biocompatibility of polyurethane SMPs has been reported in other work[43]; however, the biocompatibility of the overall design needs to be evaluated.

3. Conclusions

A new design of a magnetically actuated VSM with a silicone backbone and enclosed within deployable SMP springs is presented in this work. Variable stiffness is attained with phase change and expansion of the SMP springs. The SMP springs with embedded resistive wires are fabricated using a novel process of retraining the primary shape of SMP. The optimal dimensions of the SMP springs are determined by analyzing the bending characteristics of three VSM samples of different design parameters under magnetic actuation. Additionally, the thermal characteristics of the VSM are analyzed using 1D transient heat transfer model and infrared camera images. The coated resistive wires for Joule heating are seamlessly integrated in the VSM and proven to generate uniform thermal actuation of the SMP. As a result of preliminary design evaluations, a one-segment VSM of outer diameter 9 mm, inner diameter 2 mm, with a working length in the range 15–70 mm, and a two-segment VSM of outer diameter 10 mm, inner diameter 1 mm, with a working length in the range 25–100 mm are developed. Thus, both the VSMs are capable of fully extending their respective lengths to 4 times their fully compressed lengths. The one-segment VSM is integrated with a miniature camera and a clinically used endoscopic cold snare to demonstrate endoscopy and biopsy applications in a stomach phantom with gastric polyps. The two-segment VSM integrated with an optical fiber for laser light delivery is maneuvered to follow a sequential arrangement of three distinctly oriented rings in 3D.

The proposed concept of deployable VSM demonstrates the ability to independently actuate and bend the two segments of the VSM to form variable curvatures across varying lengths of the VSM. The variable working length of the VSM can be useful in inserting the VSM and steering to reach the target surgical site with less likelihood of deviation of the VSM from its intended path, and

subsequent expansion of the VSM enhances the range of motion and reach. Additionally, the entire shape of the VSM can be fixed which is an effective way of stabilizing the VSM while deploying laparoscopic tools through its working channel. The novel design has potential to develop a new class of smart surgical manipulators with controllable stiffness that can enhance instrument maneuverability to reach difficult-to-access surgical sites safely.

4. Experimental Section

Fabrication Method: The VSM was fabricated by assembling the silicone tube, SMP spring, and permanent magnet using flexible clamps made by 3D printing (Form 2, stereolithography printer, USA), as shown in Figure 1a. Off-the-shelf silicone tubes (Technirub International B.V., The Netherlands) and N48 neodymium ring magnets (Neomagnete, Germany) of outer diameter = 4 mm, inner diameter = 1.5 mm, and height = 1 mm were used. The SMP spring was made by first making a SMP wire having a 0.12 mm nichrome wire as the embedded resistive wire. The nichrome wire was coated with a urethane lacquer (KONTAKT 255 Urethane 71, Belgium) for insulation. The coated nichrome wire was inserted forming a loop routed inside a silicone tube of inner diameter equal to the spring wire diameter, to obtain two connection points for the current supply. The nichrome wires running though the length of the silicone tube formed an electrical circuit loop, with two ends of the nichrome wire leaving one end of the silicone tube. A potting type SMP, MP3510 (SMP Technologies Inc., Japan) which is available in two parts: resin and hardener, was used in this design. Equal amounts of resin and hardener were taken in a dual cartridge syringe gun (Adhesive Dispensing Ltd., UK) and dried using a 1 stage vacuum pump for 2 h. The resin and hardener were then mixed using a 1:1 ratio mixer nozzle and the solution was injected into the prepared silicone tube mold. The mold was immediately transferred to an oven to cure at 70 °C for 2 h. The cured SMP wire was demolded by cutting out the silicone tube. The SMP spring was obtained by retraining the SMP wire to change its primary shape to a spring shape. This was done by fixing it into a temporary shape of a spring, and heating the SMP wire above its glass transition temperature for a prolonged period of time. This is a process synonymous to annealing where the molecular disturbance due to residual strain is eliminated, as observed by a few studies which investigated the different retraining conditions of the primary shape.[44,45] The following training cycles were tested in an oven: 4 h at 70 °C + 16 h at 95 °C; 16 h at 70 °C; 4 h at 95 °C. It was found that two cycles of 16 h at 70 °C worked the best to obtain the SMP spring. The complete process of fabricating the SMP spring is illustrated in Figure 1d. Therefore, in this way the SMP spring with two nichrome wires at one end was obtained. Finally, the two nichrome wires were covered by a teflon liner of diameter 0.6 mm (Zeus Company Inc., USA) and filled with silicone rubber (Ecoflex 00-10, Smooth On Inc., USA) while leaving two short ends of the nichrome wire for electrical connection.

Stiffness Characterization: The three VSMs designed for the characterization experiments had the following number of active coils (n), inner (D_i), and outer diameters (D_o) of silicone tube, and thickness (t), inner (d_i), and outer diameters (d_o) of ring magnets: n = 3.5, 4.5, 5.5; D_o (mm) = 2.5, 3, 2.5; D_i (mm) = 1.2, 2, 1.5; t (mm) = 1, 2, 2; d_o (mm) = 4, 4, 6; d_i (mm) = 1.5, 1.5, 2; corresponding to VSM-1, VSM-2, VSM-3, respectively.

Magnetic Actuation: The stiffness characterization experiments were conducted in an electromagnetic coil setup (PaCMag), which could generate a maximum magnetic field of 55 mT.[46] The VSM was suspended in the cylindrical workspace (equal radius and height of 65 mm) and magnetic fields (B = 30 and 40 mT) were applied to deflect the manipulator. The resulting bending moment (M) acting on the VSM was given by $M = \mu \times B$, where μ is the dipole moment of the magnet attached to the VSM. Thirteen experiments each in glass and rubber phases were conducted for the three VSMs at various extended lengths and at different radial orientations of the SMP spring. Each experiment was repeated twice for bending in either direction. The deflection (θ) of the VSM was

**ADVANCED
SCIENCE NEWS**
www.advancedsciencenews.com

**ADVANCED
INTELLIGENT
SYSTEMS**
Open Access
www.advintellsyst.com

measured by a camera (FLIR Blackfly S USB3 camera, USA) which tracked the tip of the VSM.

Thermal Actuation: The heating and cooling behavior of a SMP wire of length 15 cm, SMP spring with 3.5 active coils, and VSM-1 were analyzed. Each of the samples was composed of a 0.12 mm diameter nichrome wire (resistivity $\rho = 98\,\Omega\,m^{-1}$) of length 60 cm. The thermal actuation of the three samples was done by connecting the lead wires of the SMP to a power supply (TSX3510—Precision DC Bench Power Supply, UK). Seven measurements of the temperature were taken using an infrared camera (Fluke Ti400 Infrared Camera, Washington, USA) while the samples were heated with currents 0.1, 0.2, and 0.3 A, and cooled at room temperature ($\approx 27\,°C$). The measured data were processed using the Fluke Connect software.

Applications: The one-segment VSM and two-segment VSM designs used for the demonstrations were made of one segment having 5.5 coils and two segments having 4.5 coils, respectively. Magnetic field was generated by moving a N45 neodymium disc magnet (diameter = 70 mm and height = 35 mm), which was connected to the end effector of a robot (UR5, Universal Robots, Denmark). The trajectory of the robot carrying the magnet was planned and programmed for each of the experiments. The magnet was held at a distance of 50–100 mm away from the VSM during the experiments resulting in the generation of 20–70 mT magnetic fields. For endoscopy and biopsy demonstrations, a miniature camera of diameter 0.91 mm (MD-B1000-120-01, Misumi Electronic Corporation, Taiwan) and a Diamond Cut Cold Snare of diameter 10 mm (Micro-Tech Endoscopy, China) were used. Experiments were performed in an anatomical model of the stomach (193 mm × 30 mm × 156 mm), and 3D printed elastic dome-shaped polyps of size 8 mm were glued on different locations. For laser application, a 0.2 NA 50/125 graded index multimode optical fiber (Plasma Optical Fibre B.V., The Netherlands) was integrated to the VSM. A diode-pumped solid-state laser (37-028, Edmund Optics, USA) and an objective lens 5X (M Plan Apo, Mitutoyo, Japan) were used to couple and transmit the laser light through the fiber. The three rings of inner diameters 15 mm with centers at heights of 50, 60, and 70 mm were 3D printed and were positioned with spacings of 25 and 35 mm.

Supporting Information

Supporting Information is available from the Wiley Online Library or from the author.

Conflict of Interest

The authors declare no conflict of interest.

Data Availability Statement

The data that support the findings of this study are available in the Supporting Information of this article.

[1] I. D. Walker, H. Choset, G. S. Chirikjian, *Springer Handbook of Robotics*, Springer, Würzburg, Germany **2008**, pp. 1–4.

[2] J. Burgner-Kahrs, D. C. Rucker, H. Choset, *IEEE Trans. Rob.* **2015**, *31*, 1261.

[3] M. T. Chikhaoui, J. Burgner-Kahrs, in *ACTUATOR 2018; 16th Int. Conf. New Actuators*, VDEBremen, Germany **2018**, pp. 1–11.

[4] T. da Veiga, J. H. Chandler, P. Lloyd, G. Pittiglio, N. J. Wilkinson, A. K. Hoshiar, R. A. Harris, P. Valdastri, *Prog. Biomed. Eng.* **2020**, *2*, 032003.

[5] H. B. Gilbert, D. C. Rucker, R. J. Webster III, *Rob. Res.* **2016**, *114*, 253.

[6] T. L. Thomas, V. K. Venkiteswaran, G. K. Ananthasuresh, S. Misra, *J. Mech. Rob.* **2020**, *12*, 061006.

[7] L. L. Howell, *21st Century Kinematics*, Springer, Hoboken, New Jersey, USA **2013**, pp. 189–216.

[8] X. Chen, X. Zhang, Y. Huang, L. Cao, J. Liu, *J. Field Rob.* **2022**, *39*, 281.

[9] Y. Kim, G. A. Parada, S. Liu, X. Zhao, *Sci. Rob.* **2019**, *4*, eaax7329.

[10] S. Wu, W. Hu, Q. Ze, M. Sitti, R. Zhao, *Multifunct. Mater.* **2020**, *3*, 042003.

[11] M. Richter, M. Kaya, J. Sikorski, L. Abelmann, V. Kalpathy Venkiteswaran, S. Misra, *Soft Rob.* **2023**, (in Press).

[12] Z. Wu, D. Bandara, K. Kiguchi, J. Arata, in *2019 IEEE Int. Conf. Robotics and Biomimetics (ROBIO)*, IEEE, Piscataway, NJ **2019**, pp. 2220–2224.

[13] W. Dou, G. Zhong, J. Cao, Z. Shi, B. Peng, L. Jiang, *Adv. Mater. Technol.* **2021**, *6*, 2100018.

[14] M. Brancadoro, M. Manti, F. Grani, S. Tognarelli, A. Menciassi, M. Cianchetti, *Front. Rob. AI* **2019**, *6*, 12.

[15] D. S. Shah, E. J. Yang, M. C. Yuen, E. C. Huang, R. Kramer-Bottiglio, *Adv. Funct. Mater.* **2021**, *31*, 2006915.

[16] K. Althoefer, *Nat. Rev. Mater.* **2018**, *3*, 76.

[17] M. E. Giannaccini, C. Xiang, A. Atyabi, T. Theodoridis, S. Nefti-Meziani, S. Davis, *Soft Rob.* **2018**, *5*, 54.

[18] J. Zhu, L. Lyu, Y. Xu, H. Liang, X. Zhang, H. Ding, Z. Wu, *Adv. Intell. Syst.* **2021**, *3*, 2100011.

[19] Y. Zhong, L. Hu, Y. Xu, *Actuators*, Vol. *9*, MDPI **2020**, p. 142.

[20] F. Alambeigi, R. Seifabadi, M. Armand, in *2016 IEEE Int. Conf. Robotics and Automation (ICRA)*, IEEE, Piscataway, NJ **2016**, pp. 758–764.

[21] C. Chautems, A. Tonazzini, Q. Boehler, S. H. Jeong, D. Floreano, B. J. Nelson, *Adv. Intell. Syst.* **2020**, *2*, 1900086.

[22] C. Yang, S. Geng, I. Walker, D. T. Branson, J. Liu, J. S. Dai, R. Kang, *Int. J. Rob. Res.* **2020**, *39*, 1620.

[23] M. Mattmann, C. De Marco, F. Briatico, S. Tagliabue, A. Colusso, X.-Z. Chen, J. Lussi, C. Chautems, S. Pané, B. Nelson, *Adv. Sci.* **2022**, *9*, 2103277.

[24] J. Lussi, M. Mattmann, S. Sevim, F. Grigis, C. De Marco, C. Chautems, S. Pané, J. Puigmart-Luis, Q. Boehler, B. J. Nelson, *Adv. Sci.* **2021**, *8*, 2101290.

[25] H. Jeon, Q. N. Le, S. Jeong, S. Jang, H. Jung, H. Chang, H. J. Pandya, Y. Kim, *IEEE Rob. Autom. Lett.* **2022**, *7*, 6582.

[26] Y. Cao, F. Ju, L. Zhang, D. Bai, F. Qi, B. Chen, *Proc. Inst. Mech. Eng., Part H: J. Eng. Med.* **2018**, *232*, 1098.

[27] S. Jiang, B. Chen, F. Qi, Y. Cao, F. Ju, D. Bai, Y. Wang, *Int. J. Med. Rob. Comput. Assisted Surg.* **2020**, *16*, e2081.

[28] M. C. Yuen, R. A. Bilodeau, R. K. Kramer, *IEEE Rob. Autom. Lett.* **2016**, *1*, 708.

[29] A. Lendlein, O. E. Gould, *Nat. Rev. Mater.* **2019**, *4*, 116.

[30] K. Wang, Y.-G. Jia, C. Zhao, X. Zhu, *Prog. Mater. Sci.* **2019**, *105*, 100572.

[31] Y. Piskarev, J. Shintake, C. Chautems, J. Lussi, Q. Boehler, B. J. Nelson, D. Floreano, *Adv. Funct. Mater.* **2022**, *32*, 2107662.

[32] A. M. Wahl, *Mechanical Springs*, Penton Publishing Company, Cleveland, OH **1944**.

[33] X.-J. Li, J. Yang, B.-Q. Yan, X. Zheng, in *MATEC Web of Conf.*, Vol. *175*, EDP Sciences, Guangzhou, China **2018**, p. 03014.

[34] P. S. Yarmolenko, E. J. Moon, C. Landon, A. Manzoor, D. W. Hochman, B. L. Viglianti, M. W. Dewhirst, *Int. J. Hyperthermia* **2011**, *27*, 320.

[35] M. D. Hager, S. Bode, C. Weber, U. S. Schubert, *Prog. Polym. Sci.* **2015**, *49*, 3.

[36] H. Koerner, R. J. Strong, M. L. Smith, D. H. Wang, L.-S. Tan, K. M. Lee, T. J. White, R. A. Vaia, *Polymer* **2013**, *54*, 391.

[37] A. Alteheld, Y. Feng, S. Kelch, A. Lendlein, *Angew. Chem., Int. Ed.* **2005**, *44*, 1188.

[38] M. Hallissey, W. Allum, A. Jewkes, D. Ellis, J. Fielding, *Br. Med. J.* **1990**, *301*, 513.

[39] J. Delaey, P. Dubruel, S. Van Vlierberghe, *Adv. Funct. Mater.* **2020**, *30*, 1909047.

[40] G. Baer, T. Wilson, D. Matthews, D. Maitland, *J. Appl. Polym. Sci.* **2007**, *103*, 3882.

[41] F. Carpi, C. Pappone, *Expert Rev. Med. Dev.* **2009**, *6*, 487.

[42] C. Chautems, S. Lyttle, Q. Boehler, B. J. Nelson, *IEEE Rob. Autom. Lett.* **2018**, *3*, 2123.

[43] W. Small IV, P. Singhal, T. S. Wilson, D. J. Maitland,, *J. Mater. Chem.* **2010**, *20*, 3356.

[44] H. Tobushi, D. Shimada, S. Hayashi, M. Endo, *Proc. Inst. Mech. Eng., Part L: J. Mater.: Des. Appl.* **2003**, *217*, 135.

[45] W. Small IV, T. S. Wilson, W. J. Benett, J. M. Loge, D. J. Maitland, *Opt. Express* **2005**, *13*, 8204.

[46] T. L. Thomas, J. Sikorski, G. K. Ananthasuresh, V. K. Venkiteswaran, S. Misra, *IEEE Trans. Med. Rob. Bionics* **2022**, *4*, 910.

[47] SMP Technologies Inc., http://www.smptechno.com/index_en.html (accessed: December 2022).